Research Article | Vol. 30, No. 12 / 6 Jun 2022 / Optics Express 20684
Optics EXPRESS

High-speed Ge-on-GaAs photodetector

LINZE LI,[1,2,3,7] RUI PAN,[4,7] ZHIYANG XIE,[1,2,3] YAO LU,[1,2,3] JIAXIANG CHEN,[1,2,3] XINBO ZOU,[1] ZIYUAN YUAN,[4] MENGLIN CHANG,[4] HONG LU,[4,5,8] AND BAILE CHEN[1,6,9]

[1]School of Information Science and Technology, ShanghaiTech University, Shanghai 201210, China
[2]Shanghai Institute of Microsystem and Information Technology, Chinese Academy of Sciences, Shanghai 200050, China
[3]University of Chinese Academy of Sciences, Beijing 100049, China
[4]National Laboratory of Solid State Microstructures & Department of Materials Science and Engineering, College of Engineering and Applied Sciences, Nanjing University, Nanjing 210093, Jiangsu Province, China
[5]Jiangsu Key Laboratory of Artificial Functional Materials, Nanjing University, Nanjing 210093, Jiangsu Province, China
[6]Shanghai Engineering Research Center of Energy Efficient and Custom AI IC, Shanghai 201210, China
[7]contributed equally to this work
[8]hlu@nju.edu.cn
[9]chenbl@shanghaitech.edu.cn

Abstract: In this work, a germanium (Ge) on gallium arsenide (GaAs) photodetector is demonstrated with the optical response from 850 nm to 1600 nm, which has potential for monolithic integration with VCSELs on GaAs platform as transceiver working beyond 900 nm. The device exhibits a responsivity of 0.35A/W, 0.39 A/W and 0.11 A/W at 1000 nm, 1310 nm and 1550 nm, respectively and dark current of 8 nA at -1 V. The 10 μm diameter back-illuminated device achieves a 3-dB bandwidth of 9.3 GHz under −2 V bias. A donor-like trap at the interface between the Ge and GaAs collection layers is verified by capacitance-voltage curve and deep-level transient spectroscopy (DLTS) measurement, which impedes the depletion in GaAs collection layers.

1. Introduction

High-speed, low threshold current 850 nm vertical-cavity surface-emitting lasers (VCSELs) [1] and GaAs/AlGaAs based photodetectors (PDs) with high-speed and high-efficiency performance [2,3] have been demonstrated for short-distance optical links application. The monolithic integration of GaAs-AlGaAs-based UTC-PDs and Zn-diffusion VCSELs [4], with the advantage of high data rate/power consumption ratio, can be applied in bidirectional optical interconnect techniques [5] to reduce the cost and increase the density of bus lines for data transmission. GaAs substrate with distributed Bragg reflector (DBR) based on GaAs/AlAs mixed compound has facilitated the tremendous development of VCSELs during the last few decades, which is a distinguished platform for monolithic transceiver modules [6].

To further improve the transmission capacity in short reach optical interconnect, short wavelength division multiplexing (SWDM) within the window of 850 nm to 940 nm is a promising choice [7], driving the demand for GaAs-based transceivers monolithically integrated by active devices working beyond 900 nm. However, the bandgap of GaAs is around 1.42 eV, corresponding to a cutoff wavelength of 870 nm, and it is still challenging to build active devices working beyond 900 nm due to the lack of lattice-matched material working in the corresponding band. For laser application, using strained quantum structures such as quantum dots [8] or quantum well [9] can partially solve this issue and even achieve the lasing wavelength at 1310 nm. Moreover, for detector applications, it is especially difficult to build detectors with good quantum

#459664 https://doi.org/10.1364/OE.459664
Journal © 2022 Received 28 Mar 2022; revised 25 Apr 2022; accepted 5 May 2022; published 24 May 2022

Optics EXPRESS

efficiency performance beyond 900 nm given the critical thickness limit [10] of strained quantum structure. One way to demonstrate a GaAs based detector with a response beyond 900 nm is to grow lattice-mismatch InGaAs on GaAs [11–13];However, the devices often suffer from a high dark current and require a high quality buffer layer, which is not suitable for monolithic integration to grow on the epi-layer of VCSELs.

Since Ge is nearly lattice-matched to GaAs substrate (only 0.08% mismatch), it is anticipated that Ge can be grown on GaAs platform with fewer defects as compared to InGaAs-on-GaAs and Ge-on-Si. Moreover, this bufferless Ge/GaAs integration platform could be a potential candidate for monolithic transceivers in the SWDM application, and benefits from the mature GaAs electronic technology [14], low cost and large available wafer.

In this work, we demonstrate a Ge-on-GaAs photodetector with an optical response from 850 nm to 1600 nm for the first time. The device shows optical responsivity of 0.39 A/W and 0.11 A/W at 1310 nm and 1550 nm under –1.2 V bias, respectively. The 10 μm diameter back-illuminated device achieves a 3 dB bandwidth of 9.3 GHz under –2 V bias voltage. Based on the capacitance-voltage curve and deep-level transient spectroscopy (DLTS) measurement, a donor-like trap was observed at the interface [8] between Ge and GaAs collection layers, limiting the bandwidth in terms of both RC time and carrier transit time.

2. Device design and fabrication

Figure 1 (a) and (b) show the designed epitaxial structure and energy band diagram of the Ge/GaAs UTC PD. The structure was grown on the semi-insulating GaAs substrate by a molecular beam epitaxy (MBE) system. The epitaxial growth began with a total 600 nm heavily n-doped GaAs contact layer and a 600 nm un-intentionally doped ($<1\times10^{16}$ cm^{-3}) GaAs collection layer. The partially-depleted absorption layer consists of a 200 nm un-intentionally doped Ge layer and four p-type layers with a step-grading profile (2×10^{18} cm^{-3}, 1.2×10^{18} cm^{-3}, 8×10^{17} cm^{-3}, and 5×10^{17} cm^{-3}) to form a quasi-electric field which assists electron transport. Finally, a 50 nm thick heavily p-doped Ge was deposited as a contact layer. After the growth of epi-layer, in-situ annealing process at 500 °C was conducted to improve the crystal quality. To further verify the quality of the Ge on GaAs, we compared the X-ray diffraction (XRD) result of the Ge/GaAs epi-layer to the Ge on Si control samples in-situ annealed at different temperatures, as shown in Fig. 2. It is clear shown in Fig. 2 that the full widths at half maximum (FWHM) of XRD of the Ge epi-layer on GaAs substrate is much smaller than that of the Ge/Si sample under various in-situ annealing temperatures, indicating a better Ge film quality on GaAs compared to growing Ge on Si.

The device was fabricated into a double-mesa structure, as shown in Fig. 1 (c). The first mesa was stopped at the GaAs n-contact layer by an inductively coupled plasma (ICP) dry etch process. The second mesa was terminated at the semi-insulating GaAs substrate by wet etch (H_3PO_4:H_2O_2:H_2O = 1:1:10) to ensure electrical isolation between devices. Ti/Pt/Au and GeAu/Ni/Au were deposited on the p-type and n-type contact layers by electron beam evaporation, respectively. A good ohmic contact was formed by the rapid thermal annealing process. Then a 265 nm silicon oxide film as an anti-reflection (AR) coating was deposited to decrease the reflection at 1.55 μm wavelength by using plasma-enhanced chemical vapor deposition (PECVD). The photodiodes were connected to gold-plated coplanar waveguide (CPW) pads of 50 Ω characteristic impedance through an air-bridge.

Optics EXPRESS

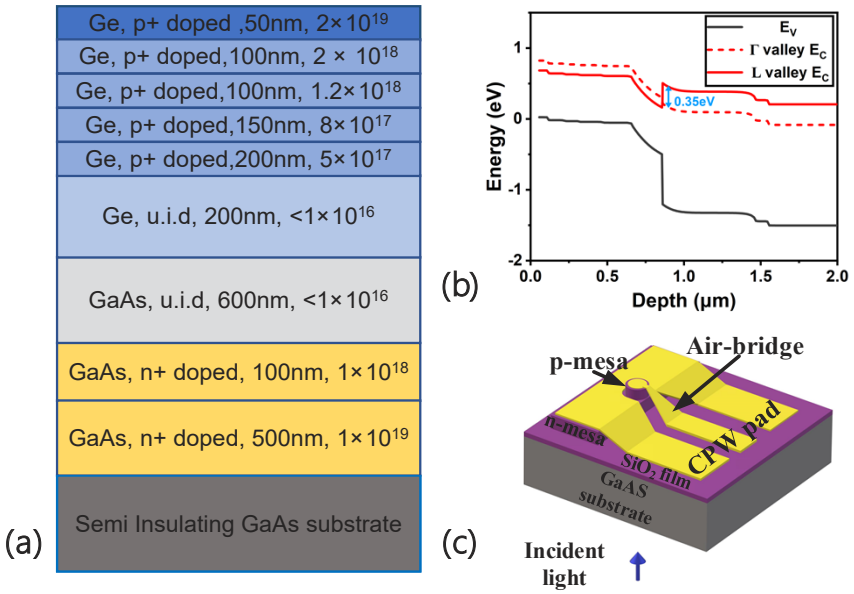

Fig. 1. (a) Epi-layer structure of the Ge/GaAs UTC. (b) Equilibrium energy band diagram of Γ valley and L valley of designed devices. (c) Schematic diagram of the fabricated back-illuminated device.

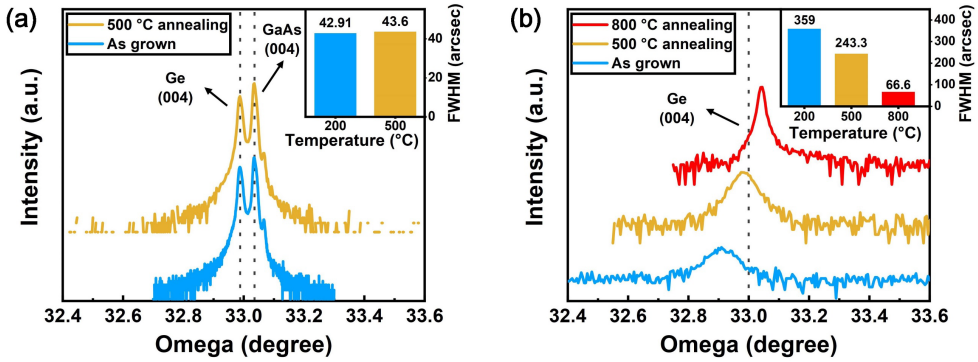

Fig. 2. XRD spectra of the omega-two theta scans on the (004) plane of (a) Ge on GaAs epi-layer and (b) Ge on Si samples annealed at different temperatures. The insert shows the FWHM of the Ge (004) peak as a function of annealing temperatures.

Optics EXPRESS

3. DC electrical characterization

The dark current versus bias voltage characteristics for devices with diameters from 10 µm to 34 µm at room temperature are shown in Fig. 3 (a). Under −2 V bias, typical dark currents range from 10^{-8} to 10^{-7} A, the corresponding dark current density for the 20 µm diameter device under −1 V bias at room temperature is 3.8 mA/cm^2. The dark current density versus periphery/area (P/A) is shown in Fig. 3 (b). The intercept of the linear fit corresponds to a bulk current density much lower than the total dark current density for all devices with different diameters, indicating that the surface leakage current is dominant, which could be attributed to the sidewall damage caused by dry etch process.

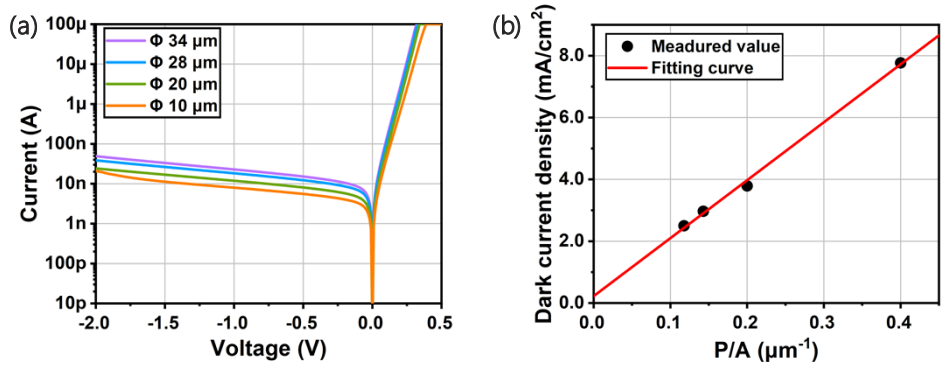

Fig. 3. (a) Dark current versus bias voltage characteristic for devices with various diameters at room temperature. (b) Dark current density as a function of P/A under −1 V bias and linear fit.

The temperature-dependent dark current-voltage characteristics of the 20 µm diameter device at different temperatures from 150 to 300 K are shown in Fig. 4 (a). Linear fit of the Arrhenius plot (see Fig. 4(b)) under −1 V bias shows an activation energy () of 0.144 eV, which is much lower than half of the effective bandgap (E_g= 0.729 eV) of the Ge absorber, verifying the surface leakage dark current mechanism from another perspective.

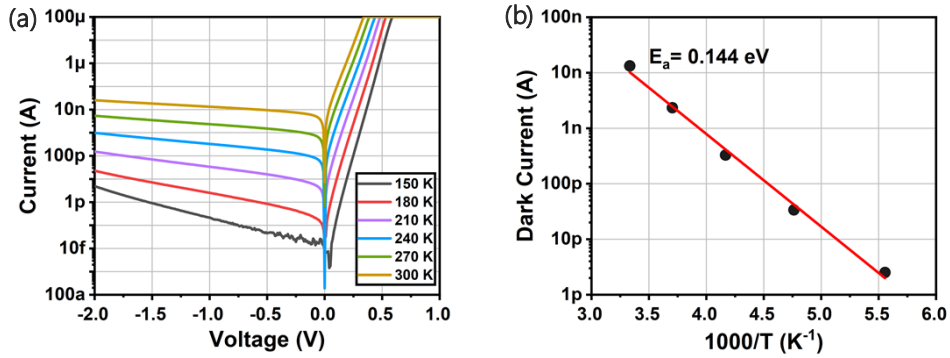

Fig. 4. (a) Dark current-voltage characteristics of the 20 µm diameter device at different temperatures from 150 to 300 K. (b) Arrhenius plot of the dark current under −1 V bias.

Figure 5 (a) shows the capacitance-voltage characteristic of UTC PDs at room temperature. The photodiode capacitance (C_{PD}), composed of junction capacitance (C_{pn}) and parasitic capacitance (C_{st}), initially decreases and then saturates when the un-intentionally doped regions are fully depleted (above 0.5 V reverse bias). A C_{st} of 67.3 fF was found by plotting the C_{PD} versus

Optics EXPRESS

device areas, determined from the intercept of the linear fit, as shown in Fig. 5 (b). The parasitic capacitance might originate from the air-bridge and CPW line by the electroplating process [15].

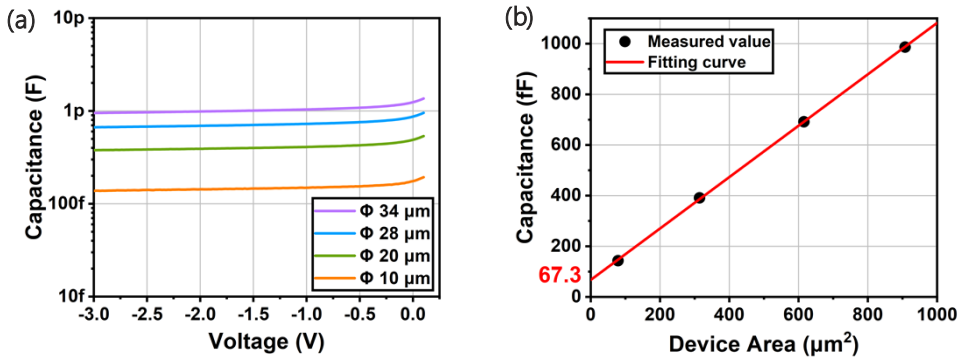

Fig. 5. (a) Measured capacitance versus reverse bias characteristics at room temperature. (b) Capacitance of devices under −2 V bias and linear fit.

4. Responsivity and detectivity

The responsivity of a top-illuminated 500 μm diameter device was measured by comparing the photocurrent collected by a lock-in amplifier with a calibrated commercial Ge photodiode. Monochromatic light ranging from 850 nm to 1700nm was produced by a tungsten lamp with a broadband spectrum followed by the grating spectrometer. The responsivity as a function of wavelength is shown in Fig. 6. The responsivity of the device at 1310 nm is 0.39 A/W under zero bias. The device exhibits a slight increase of responsivity at 1550 nm from 0.1 A/W to 0.11 A/W as the bias voltage varies from 0 V to −1.2 V. Larger reverse bias voltage would introduce considerable dark currents, affecting extraction of the optical response through the lock-in amplifier. Based on the absorption coefficient of Ge film on the epitaxial wafer, which was measured by ellipsometer (see Fig. 7), the carrier collection efficiency at 1310 nm under −1.2 V bias is estimated to be 75.7%; however, it is only 41.1% at 1550 nm even with a perfect antireflection coating at this wavelength. That is because most of the photogenerated electrons by 1550 nm light are created in the L valley of Ge. Unlike the smooth conduction band energy (*Ec*) in the Γ valley, a band offset of 0.35 eV was found at the Ge/GaAs heterointerface in the L valley, as shown in Fig. 1 (b), limiting the collection of photogenerated carriers at 1550 nm wavelength.

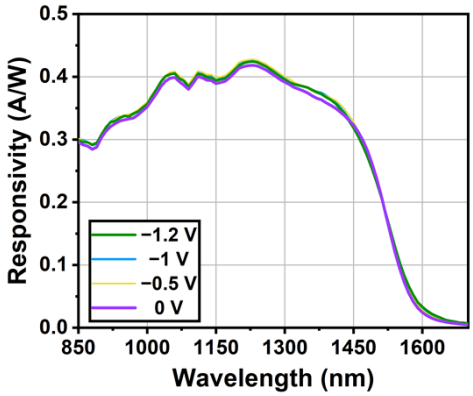

Fig. 6. Responsivity of a 500 μm diameter device at various bias voltages.

Optics EXPRESS

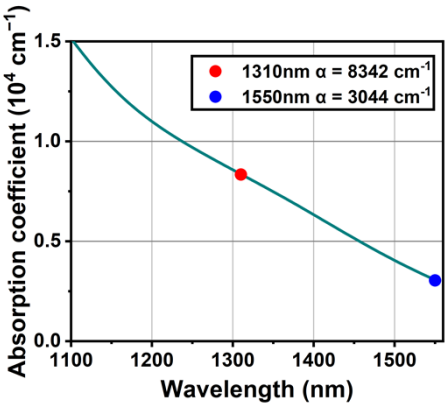

Fig. 7. Absorption coefficient of Ge versus wavelength.

To evaluate the overall performance, the current noise of the 500 µm device was measured at −0.5 V by a noise spectrum analyzer inside a shield, as shown in Fig. 8. The theoretical white noise spectral density is also depicted in Fig. 8, according to:

$$\frac{i_n^2}{\Delta f} = 2qI + \frac{4kT}{R_e} \tag{1}$$

where k, T, R_e, q and I represent the Boltzmann constant, temperature in K, differential resistance, electron charge, and the dark current. The measured current noise is close to the calculated white noise in the high frequency regime, while it is several orders higher in the low frequency regime due to the existence of $1/f$ noise.

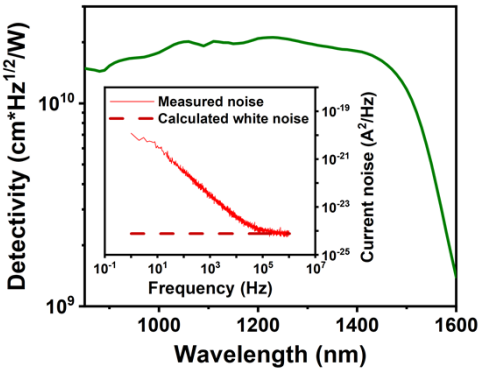

Fig. 8. The calculated detectivity of the 500 µm diameter device measured at −0.5 V bias. The insert shows the current noise power spectral densities as a function of frequency measured at −0.5 V bias (solid line) and white noise calculated by Eq. (1) (dash line).

The white noise-limited detectivity (D^*) is determined from [16]:

$$D^* = \frac{R\sqrt{A}}{\sqrt{i_n^2/\Delta f}} \tag{2}$$

where R is the responsivity, A is the area of device. As shown in Fig. 8, the calculated D^* of the device under −0.5 V bias reaches 1.92×10^{10} cm·Hz$^{1/2}$/W and 5.16×10^9 cm·Hz$^{1/2}$/W at 1310 nm and 1550 nm, respectively.

Optics EXPRESS

5. Radio frequency characterization

The frequency response of the Ge/GaAs UTC device was investigated by a calibrated lightwave component analyzer (LCA) system [3]. The modulated optical signal at 1550 nm wavelength generated by the LCA system was coupled into the device by a lensed fiber. Then the RF signal was collected by the LCA system through a GSG probe, while the DC bias was provided by the source meter through a bias tee. During the bandwidth measurement, the lensed fiber was pulled back to a point where the responsivity dropped by 50% to ensure uniform illumination. Frequency-dependent loss value introduced by cables and GSG probe was calibrated by a vector network analyzer (VNA).

Theoretically, the 3 dB bandwidth of the photodiode is limited by transit time and RC time, as expressed by the equation [15]:

$$\frac{1}{f_{3dB}{}^2} = \frac{1}{f_{RC}{}^2} + \frac{1}{f_{tr}{}^2} \tag{3}$$

where f_{3dB} ., f_{RC} ., f_{tr} . are the total 3-dB bandwidth, RC-limited bandwidth, and the transit-time-limited bandwidth, respectively. The frequency response of back-illuminated devices with diameters from 10 µm to 34 µm under 0 V and −2 V bias is shown in Fig. 9. For the 10 µm diameter device, the 3 dB bandwidth grows from 7.3 GHz to 9.3 GHz when the reverse bias rises from 0 V to −2 V, which is attributed to the increasing electric field in the depletion region. The device with diameter of 34 µm, 28 µm and 20 µm shows a 3-dB bandwidth of 2.3 GHz, 3.2 GHz and 5.0 GHz under −2 V bias, respectively.

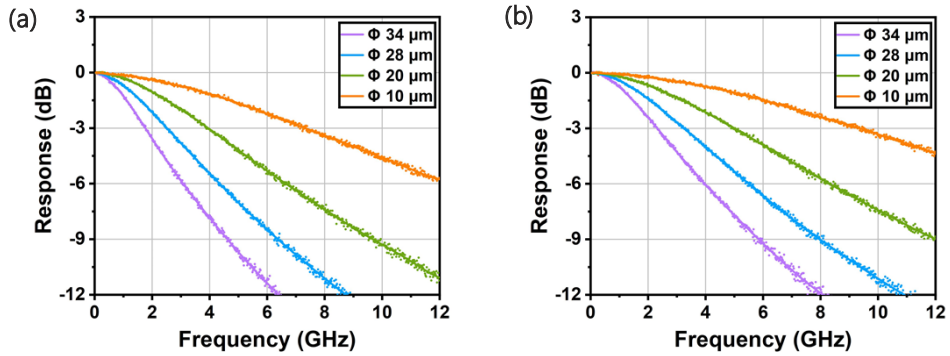

Fig. 9. Frequency response of the device with different diameters under (a) zero bias and (b) −2 V bias.

To further investigate the bandwidth limiting factor of devices, the scattering parameters (S11) of UTC-PDs were measured by VNA. Parameter fitting was conducted in Advanced Design System (ADS) stware with the equivalent circuit as depicted in Fig. 10, where R_s., R_p. and L_s. represent the series resistance, junction resistance and series inductance, respectively.

The fitting curves and the measured S11 data in the shart under −2 V are shown in Fig. 11. The corresponding extracted data along with the measured C_{PD}. (see Fig. 5 (a)) are summarized in Table 1. The fitted junction resistance (R_p.), typically on the order of 250 MΩ, is not listed in the table. From Table I, the extracted total capacitance (C_{PD}), which is closely related to the depletion width, shows good agreement with the measured value. Here the C_{PD} is relatively large compared to ideal PDs with a depletion region width of 800 nm and the same 67.3 fF C_{st} extracted in Fig. 5 (b) (204 fF theoretical C_{pd} for a 34 µm diameter device). The designed depletion region consists of a 200 nm un-intentionally doped Ge layer and a 600 nm GaAs collection layer. The depletion

Optics EXPRESS

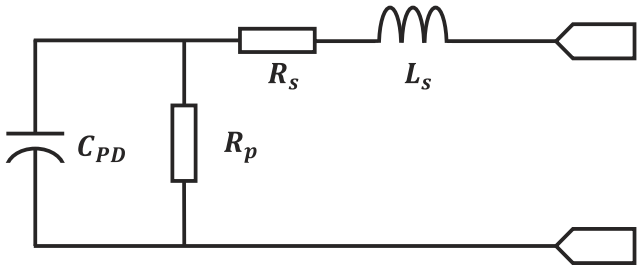

Fig. 10. Equivalent circuit model of the UTC device for S11 fitting.

width could be derived from C_{pn} by an analytical equation:

$$d = \frac{\varepsilon_0 \varepsilon_r A}{C_{pn}} \tag{4}$$

where ε_0, ε_r and A are the permittivity of free space, the dielectric constant of the depleted region, and active area of the photodiode, respectively.

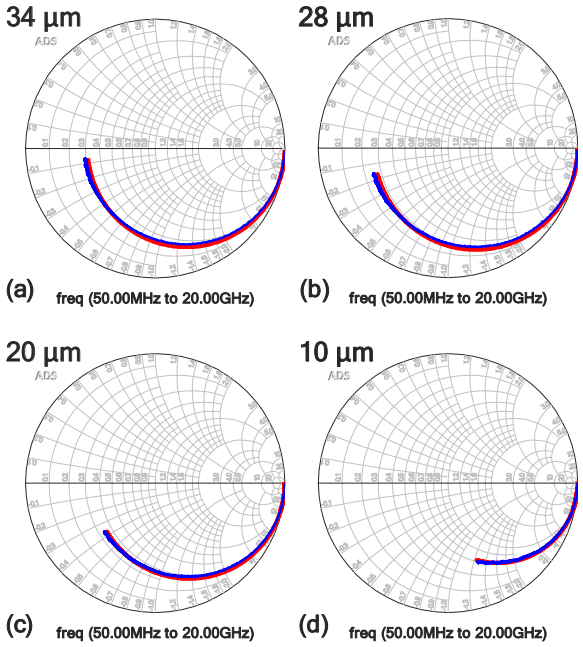

Fig. 11. Measured (blue line) and fitted (red line) S11 data of (a) 34 μm, (b) 28 μm, (c) 20 μm and (d) 10 μm devices with 50 MHz-20 GHz frequency range under −2 V bias.

Figure 12 shows the calculated depletion width versus bias voltage of a 10 μm diameter device. As the reverse bias voltage increases, the depletion width approaches 195 nm, indicating that only un-intentionally-doped (uid) Ge layer can actually be depleted. In order to study the phenomenon, deep-level transient spectroscopy (DLTS) test was conducted to observe the electrically active defects. From the DLTS spectra at −1.5 V reverse bias voltage along with the Arrhenius plot of detected traps, as shown in Fig. 13, a donor-like trap (E_1) with an energy level near E_C − 0.1 eV and concentration of 1.13×10^{16} cm^{-3} is observed. During the measurement process, the

Optics EXPRESS

Table 1. Measured and fitted parameters

Diameter (μm)	Rs (Ω)	Ls (pH)	C_{PD} (fF)	measured C_{PD} (fF)
34	15.7	43.3	945.3	957.1
28	13.7	33.6	653.8	666.0
20	17.7	27	370.9	377.8
10	31	11.6	125.1	132.2

capacitance transients started to be observed clearly as the reverse bias voltage (U_R) increased to above −1 V, while keeping a constant filling pulse voltage ($U_p = 0.05$ V), filling pulse time ($t_p = 10$ ms) and period width ($T_w = 180$ ms). The increase of reverse bias corresponded to the extension of depletion region towards the interface between Ge and GaAs collection layers, revealing that the donor-like trap was formed during the MBE growth process near the interface. Thus, the length of the equivalent junction shrinks from the expected 800 nm to around 200 nm, leading to decreases in RC-limited bandwidth. Moreover, the un-depleted 600 nm uid-GaAs also degrades the transit-time-limited bandwidth.

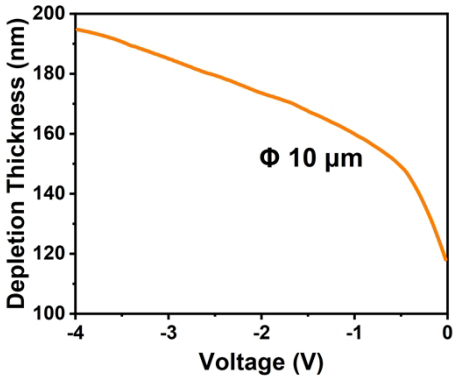

Fig. 12. Calculated depletion width of the 10 μm diameter device.

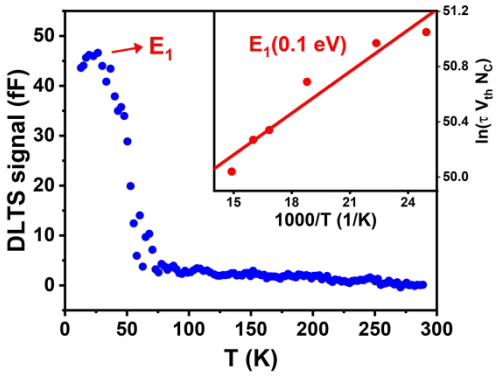

Fig. 13. DLTS spectra showing $E_V - 0.1$ eV trap level at −1.5 V bias voltage. The insert shows the Arrhenius plot of the electron trap detected in the DLTS measurement.

Figure 14 shows the calculated RC-limit frequency response using the equivalent circuit model. The RC-limit bandwidth of devices with diameters from 34 μm to 10 μm under −2 V bias is only

Optics EXPRESS

2.6 GHz, 3.9 GHz, 6.4 GHz, and 15.9 GHz, respectively. It can be attributed to the defect-induced large junction capacitance as analyzed, which is proportional to the device area as well.

According to Eq. (1), the transit-time-limited bandwidth is determined to be 9.8 GHz from the intercept of the linear fit by plotting $1000/f_{3dB}{}^2$ versus $1000/f_{RC}{}^2$ (see Fig. 15). Transit-limit process limits the overall bandwidth of the 10 μm device since f_{tr} is lower than f_{RC}. For devices with lager diameters, the bandwidth exhibits a strong dependency on size and f_{tr} is larger than f_{RC}, which is dominated by RC limit. A comparison of the simulated electric field of the device with and without donor-like trap under high reverse bias is depicted in Fig. 16 (a). The un-depleted GaAs collection layer for the device with donor-like trap can be observed, where an unexpected lower electric field would result in a longer carrier transit time compared to the fully depleted GaAs collector for the device without such interface trap. Considering the high mobility (about 6000 cm^2/Vs) of electrons in GaAs, such low electric field can still provide a drift velocity even under zero bias, as shown in Fig. 16 (b). Moreover, the diffusion process of electron could help to achieve a reasonable speed. As reverse bias increases, the depletion region slightly extends towards Ge absorption region and accelerates the carrier transport, leading to only a slightly shorter transit time.

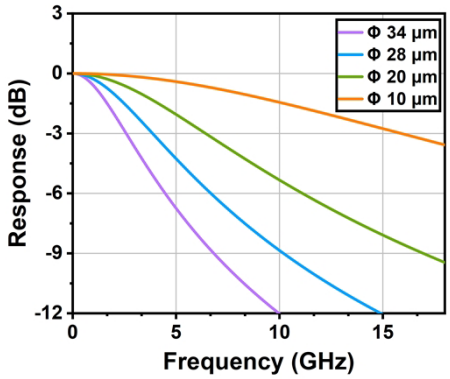

Fig. 14. Calculated RC-limit frequency response using the equivalent model with the extracted parameters.

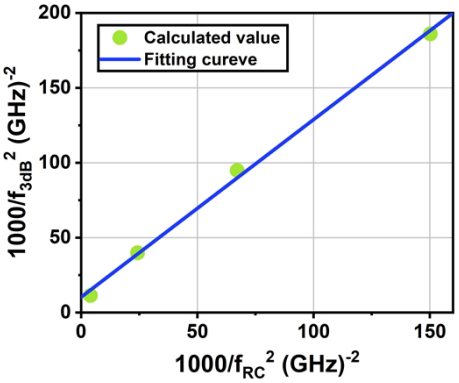

Fig. 15. Calculated $1000/f_{3dB}{}^2$ versus $1000/f_{RC}{}^2$ under −2 V bias and linear fit.

Table 2. shows the performance of the devices in this work compared to the other vertical-illumination Ge/Si PDs with a similar absorption region thickness and bulk Ge PDs. Compared

Optics EXPRESS

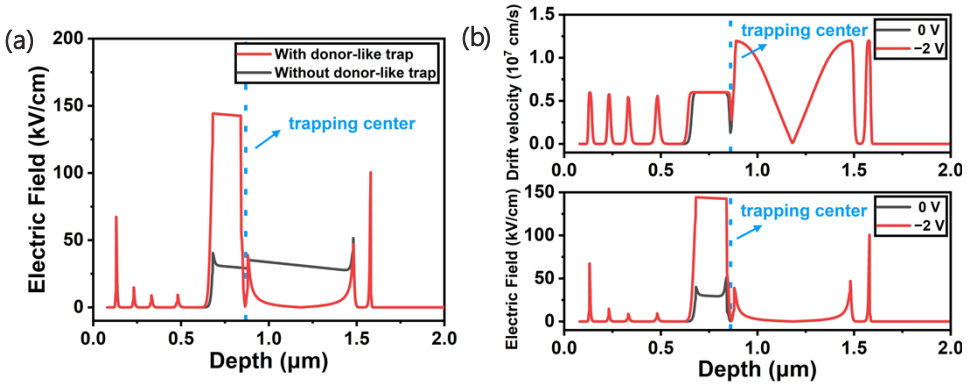

Fig. 16. (a) Simulated electric field of the device with and without donor-like trap under −2 V. (b) Simulated electric field and Drift velocity of the device with donor-like trap under different bias.

with bulk Ge PDs [17], the Ge/GaAs UTC PDs in this work have higher 3 dB bandwidth and comparable dark current density, but lower responsivity limited by active layer thickness. Compared with Ge/Si PDs, our devices have a comparable responsivity and at least 1-order lower dark current density. The bandwidth of our device is still comparable to works in Ref. [18,19] and is lower than the Ge/Si UTC PD in Ref. [20] due to the donor-like trap in the Ge/GaAs interface, which would hinder the expansion of depletion region towards GaAs and lead to lower bandwidth.

Table 2. Performance comparison with Ge/Si PDs and Ge/Ge PDs

Ref	Device structure	Absorber thickness (nm)	Responsivity (A/W)	Dark current density (mA/cm^2)	3dB bandwidth (GHz)
[17]	Ge/Ge p-n	NA	0.46 @ 1550 nm (0 V)	5.4 (−1 V)	0.19 (0 V)
[18]	Ge/Si UTC on SOI substrate	600	0.18 @ 1550 nm (−1 V)	96.3 (15 μm diameter) 61.9 (40 μm diameter) (−1 V)	9.72 (−5 V)
[19]	Ge/Si p-i-n	800	0.4 @ 1310 nm 0.2 @ 1550 nm (0 V)	200 (−1 V)	10 (NA)
[20]	Ge/Si UTC	800	0.29 @ 1310 nm 0.12 @ 1550 nm (−1 V)	35 (−1 V)	20 (−2 V)
This work	Ge/GaAs UTC	800	0.35 @ 1000 nm 0.39 @ 1310 nm 0.11 @ 1550 nm (−1 V)	2.3 (34 μm diameter) 3.8 (20 μm diameter) 7.8 (10 μm diameter) (−1 V)	9.3 (−2 V)

Considering the impact of the interfacial donor-like trap on devices performance, further optimization of the growth of Ge epitaxial films on GaAs is needed to improve the performance

Optics EXPRESS

of the devices. Another approach to eliminating the influence of such trap is to design a Ge partially depleted absorber (PDA) photodetector on GaAs substrate. PDA structure with Ge depleted absorber sandwiched between Ge P-doped and n-doped absorber, can achieve good high-speed performance with properly designed layer thickness to balance to the transit time of electrons and holes [21]. Additionally, the homojunction structure can get rid of the issue of Ge/GaAs heterointerface in the depletion region and remove band discontinuities, which is expected to have better high-speed and responsivity performance.

6. Conclusion

In this work, we have reported Ge/GaAs based high-speed UTC PDs operating at 1550 nm wavelength with a typical responsivity of 0.1 A/W. The 3 dB bandwidths under zero bias and −2 V bias of the 10 μm devices is 7.3 GHz and 9.3 GHz, respectively. According to analysis based on capacitances fitting and DLTS test, a donor-like trap is located at the interface between Ge and GaAs collection layers, leading to a significant reduction in both RC-limit bandwidth and transit-time-limit bandwidth. This work also provides directions for further devices optimization to reduce the influence of the donor-like trap, and has promising applications for SWDM transceivers.

Funding. National Key Research and Development Program of China (2018YFB2201000); National Natural Science Foundation of China (61975121).

Acknowledgments. We are grateful to the device fabrication support from the ShanghaiTech University Quantum Device Lab.

Disclosures. The authors declare no conflicts of interest.

Data availability. Data underlying the results presented in this paper are not publicly available at this time but may be obtained from the authors upon reasonable request.

References

1. J. W. Shi, J. C. Yan, J. M. Wun, J. Chen, and Y. J. Yang, "Oxide-Relief and Zn-Diffusion 850-nm Vertical-Cavity Surface-Emitting Lasers With Extremely Low Energy-to-Data-Rate Ratios for 40 Gbit/s Operations," IEEE J. Sel. Top. Quantum Electron. **19**(2), 7900208 (2013).
2. F. Kuo, T. Hsu, and J. Shi, "A GaAs/AlGaAs based uni-traveling-carrier photodiode for 10Gbit/sec optical interconnect at 850 nm wavelength with zero electrical power consumption," in *2009 Conference on Optical Fiber Communication*, 2009), 1.
3. Z. Xie, Z. Zhou, L. Li, Z. Deng, H. Ji, and B. Chen, "High-Speed 850 nm Photodetector for Zero-Bias Operation," IEEE J. Sel. Top. Quantum Electron. **28**(2), 1–7 (2022).
4. J. Shi, F. Kuo, T. Hsu, Y. Yang, A. Joel, M. Mattingley, and J. Chyi, "The Monolithic Integration of GaAs–AlGaAs-Based Unitraveling-Carrier Photodiodes With Zn-Diffusion Vertical-Cavity Surface-Emitting Lasers With Extremely High Data Rate/Power Consumption Ratios," IEEE Photonics Technol. Lett. **21**(19), 1444–1446 (2009).
5. C. L. Schow, F. E. Doany, O. Liboiron-Ladouceur, C. Baks, D. M. Kuchta, L. Schares, R. John, and J. A. Kash, "160-Gb/s, 16-Channel Full-Duplex, Single-Chip CMOS Optical Transceiver," in *OFC/NFOEC 2007 - 2007 Conference on Optical Fiber Communication and the National Fiber Optic Engineers Conference*, 2007), 1–3.
6. A. Kern, S. Paul, D. Wahl, A. Al-Samaneh, and R. Michalzik, "Single-Fiber Bidirectional Optical Data Links with Monolithic Transceiver Chips," Adv. Opt. Technol. **2012**, 1–8 (2012).
7. Y. Liu, L. Ma, W. Xiao, R. Wang, J. Xiong, J. Luo, and Z. He, "Wideband multimode fiber with an optimized core size and fluorine-doped cladding for high-speed SWDM and CWDM transmission," Opt. Express **27**(11), 15433–15443 (2019).
8. F. Hopfer, A. Mutig, M. Kuntz, G. Fiol, D. Bimberg, N. Ledentsov, V. Shchukin, S. Mikhrin, D. Livshits, and I. Krestnikov, "Single-mode submonolayer quantum-dot vertical-cavity surface-emitting lasers with high modulation bandwidth," Appl. Phys. Lett. **89**(14), 141106 (2006).
9. V. Gambin, W. Ha, M. Wistey, H. Yuen, S. R. Bank, S. M. Kim, and J. S. Harris, "GaInNAsSb for 1.3-1.6-μm-long wavelength lasers grown by molecular beam epitaxy," IEEE J. Sel. Top. Quantum Electron. **8**(4), 795–800 (2002).
10. S. Xiaoguang, W. Shuling, J. S. Hsu, R. Sidhu, X. G. Zheng, L. Xiaowei, J. C. Campbell, and A. L. Holmes, "GaAsSb: a novel material for near infrared photodetectors on GaAs substrates," IEEE J. Sel. Top. Quantum Electron. **8**(4), 817–822 (2002).
11. L. Zimmermann, J. John, S. Degroote, G. Borghs, C. Van Hoof, and S. Nemeth, "Extended wavelength InGaAs on GaAs using InAlAs buffer for back-side-illuminated short-wave infrared detectors," Appl. Phys. Lett. **82**(17), 2838–2840 (2003).

Optics EXPRESS

12. F. E. Ejeckam, C. L. Chua, Z. H. Zhu, Y. H. Lo, M. Hong, and R. Bhat, "High-performance InGaAs photodetectors on Si and GaAs substrates," Appl. Phys. Lett. **67**(26), 3936–3938 (1995).
13. L. F. Lester, K. C. Hwang, P. Ho, J. Mazurowski, J. M. Ballingall, J. Sutliff, S. Gupta, J. Whitaker, and S. L. Williamson, "Ultrafast long-wavelength photodetectors fabricated on low-temperature InGaAs on GaAs," IEEE Photonics Technol. Lett. **5**(5), 511–514 (1993).
14. C. P. Dietrich, A. Fiore, M. G. Thompson, M. Kamp, and S. Höfling, "GaAs integrated quantum photonics: Towards compact and multi-functional quantum photonic integrated circuits," Laser Photonics Rev. **10**(6), 870–894 (2016).
15. Y. Chen, Z. Xie, J. Huang, Z. Deng, and B. Chen, "High-speed uni-traveling carrier photodiode for 2 μm wavelength application," Optica **6**(7), 884 (2019).
16. Z. Deng, D. Guo, C. González Burguete, J. Huang, Z. Xie, H. Liu, J. Wu, and B. Chen, *Demonstration of Si based InAs/GaSb type-II superlattice p-i-n photodetector* (2019).
17. Y. Bao, K. Sun, N. Dhar, and M. Gupta, "Germanium p-n Junctions by Laser Doping for Photonics/Microelectronic Devices," IEEE Photonics Technol. Lett. **26**(14), 1422–1425 (2014).
18. L. Colace, M. Balbi, G. Masini, G. Assanto, H.-C. Luan, and L. C. Kimerling, "Ge on Si p-i-n photodiodes operating at 10Gbit/s," Appl. Phys. Lett. **88**(10), 101111 (2006).
19. C. Li, C. Xue, Z. Liu, H. Cong, B. Cheng, Z. Hu, X. Guo, and W. Liu, "High-responsivity vertical-illumination Si/Ge uni-traveling-carrier photodiodes based on silicon-on-insulator substrate," Sci. Rep. **6**(1), 27743 (2016).
20. M. Piels and J. Bowers, "Si/Ge uni-traveling carrier photodetector," Opt. Express **20**(7), 7488–7495 (2012).
21. S. Demiguel, X. Li, N. Li, H. Chen, J. C. Campbell, J. Wei, and A. Anselm, "Analysis of Partially Depleted Absorber Waveguide Photodiodes," J. Lightwave Technol. **23**(8), 2505–2512 (2005).